ACS MATERIALS LETTERS

www.acsmaterialsletters.org

LETTER

Machine-Learning-Driven Discovery of Mn^{4+}-Doped Red-Emitting Fluorides with Short Excited-State Lifetime and High Efficiency for Mini Light-Emitting Diode Displays

Hong Ming, Yayun Zhou,* Maxim S. Molokeev, Chuang Zhang, Lin Huang, Yuanjing Wang, Hong-Tao Sun, Enhai Song,* and Qinyuan Zhang*

Cite This: *ACS Materials Lett.* 2024, 6, 1790−1800

Read Online

ACCESS | Metrics & More | Article Recommendations | Supporting Information

ABSTRACT: **The discovery of high-efficiency Mn^{4+}-activated fluoride red phosphors with short excited-state lifetimes (ESLs) is urgent and crucial for high-quality, wide-color-gamut display applications. However, it is still a great challenge to design target phosphors with both short ESL and high luminescence efficiency. Herein, we propose an efficient machine learning approach based on a small dataset to establish the ESL prediction model, thereby facilitating the discovery of new Mn^{4+}-activated fluorides with short ESLs. Such a model can not only accurately predict the ESLs of Mn^{4+} in fluorides but also quantify the impact of structure features on ESLs, therefore elucidating the "structure-lifetime" correlations. Guided by the correlations, two new Mn^{4+}-doped tetramethylammonium (TMA)-based hybrid fluorides $(TMA)_2BF_6:Mn^{4+}$ (B = Sn or Hf) with both short ESLs ($\tau \leq 3.7$ ms) and high quantum efficiencies (internal QEs > 92%, external QEs > 55%) have been discovered successfully. A prototype displayer with excellent performance (~124% National Television Standards Committee (NTSC) color gamut) is assembled by employing a $(TMA)_2SnF_6:Mn^{4+}$-based white Mini-LED backlight module, demonstrating its practical prospects in high-quality displays. This work not only brings promising candidates for Mn^{4+}-doped fluoride phosphors but also provides a valuable reference for accelerating the discovery of new promising phosphors.**

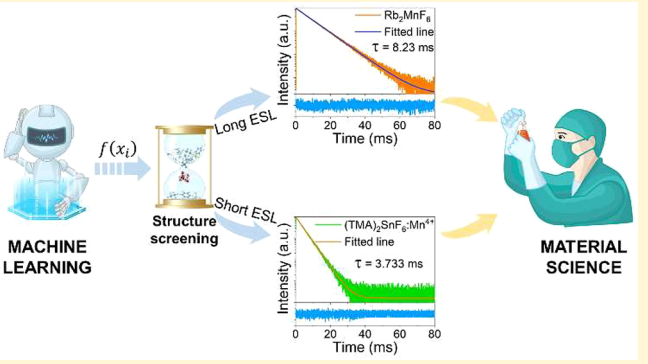

Mn^{4+}-activated fluorides are potential red converter candidates for phosphor-converted white light-emitting diodes (pc-WLED) due to their fascinating luminescent properties (e.g., narrow-band emission) and low-cost advantage of being rare-earth-free, which endow them with great competitiveness in high-quality wide color gamut display.[1,2] However, they generally suffer from long excited-state lifetimes (ESLs > 5 ms, e.g., ~8 ms for commercial $K_2SiF_6:Mn^{4+}$ (KSF)) due to the spin- and parity-forbidden characteristics of Mn^{4+}:$^2E \rightarrow {}^4A_2$ transition.[3] Such long ESLs will not only induce the nonthermal optical saturation under high-power excitation, but also lead to the red trailing smear or motion blur problems, showing adverse effects on the image quality of backlight display (particularly in high-definition displays based on Mini-LEDs).[4,5] The long ESL has become the Achilles' heel of Mn^{4+}-doped fluoride red phosphors. Therefore, there is an urgent need to discover Mn^{4+}-activated fluorides with short ESLs.

Currently, there have been some reports on Mn^{4+}-activated fluorides with short ESLs, which are mainly designed by heterovalent doping of Mn^{4+} into the fluoride matrixes represented by $K_2NbF_7:Mn^{4+}$.[6] However, their internal and external quantum efficiencies (IQEs and EQEs) are inferior due to the luminescence quenching caused by charge compensation defects.[7] In other words, this short ESL is achieved at the expense of the luminescence efficiency. Compared to heterovalent doping systems, the equivalent counterparts represented by KSF do not suffer from charge compensation defects, so they

Received: February 4, 2024
Revised: March 13, 2024
Accepted: March 19, 2024

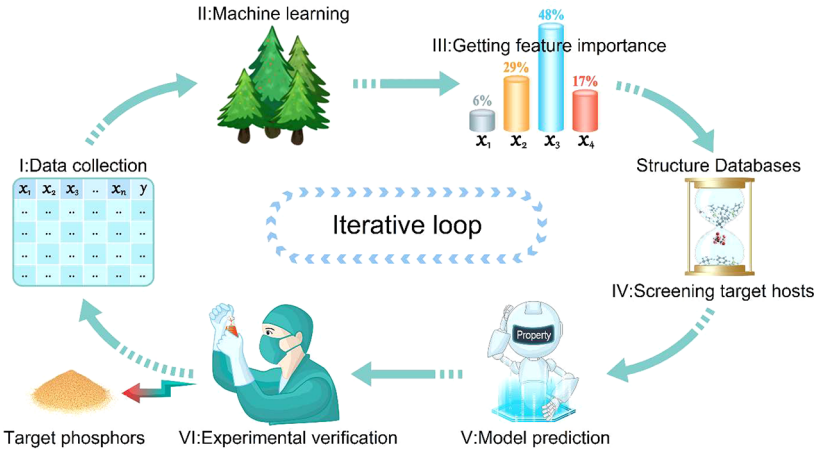

Figure 1. Schematic machine learning-driven strategy for discovering Mn^{4+}-doped fluoride phosphors with desired ESLs. An iteration includes six steps, i.e., (I) data collection, (II) machine learning, (III) getting feature importance, (IV) screening target hosts from structure databases, (V) model prediction, and (VI) experimental verification.

generally possess higher IQEs and EQEs but longer ESLs.[8] Therefore, it is still a huge challenge to design Mn^{4+}-activated fluorides with both high efficiency and short ESL.

Considering the principle that structure determines properties, the prerequisite for achieving a short ESL is to reveal the "structure-lifetime" correlations between fluoride matrixes and Mn^{4+}. In recent years, data-driven machine learning (ML) has been proven to be an effective tool for accelerating the discovery of new materials.[9,10] The state of the art in phosphor research has also begun to focus on ML for the prediction of properties and the optimization of synthesis parameters.[11] This led to the accelerated discovery of new phosphors with desirable luminescent properties. Nevertheless, utilizing ML to unveil the "structure−property" relationship between host matrixes and activators has not received the attention it deserves. Given that the electronic transitions of Mn^{4+} rely on the crystal field environment provided by the host structure,[12] we therefore took the view that such "structure−lifetime" relationship could greatly facilitate the discovery and screening of new promising Mn^{4+}-doped fluorides with short ESLs. In addition, our previous research on Mn^{4+}-doped organic−inorganic hybrid (oxy)-fluorides has demonstrated that the key to achieving high luminescence efficiency is the highly isolated octahedral lattice framework in the matrix, which can effectively avoid the agglomeration of Mn^{4+} and suppress the energy transfer of Mn^{4+}−Mn^{4+} and Mn^{4+}-to-defects.[3,13] Combining this structural feature with the "structure−lifetime" correlations to be unveiled, we can rationally design Mn^{4+}-activated fluorides that possess both short ESL and high QEs.

Nowadays, the community of Mn^{4+}-activated fluoride phosphors,[14] including all-inorganic and organic−inorganic hybrid systems, has accumulated enough cases for ML.[15] Accordingly, in this work, we employ the ML strategy on Mn^{4+}-doped fluoride phosphors to unveil the "structure−-lifetime" correlations between fluoride matrixes and Mn^{4+}, thereby guiding the discovery of new Mn^{4+}-activated fluorides with both short ESL and high QEs. By training on a small dataset of 40 cases, we build a reliable ML model that is not only able to accurately predict the ESLs of Mn^{4+} in fluorides, but also reveals the "structure−lifetime" correlations between the fluoride matrix and Mn^{4+}. Moreover, the relationship between energy levels and ESLs of Mn^{4+} was studied in detail, where the luminescence decay mechanism for the long/short ESL controlled by the structural parameters was unraveled. Guided by these correlations, two new Mn^{4+}-activated organic−inorganic hybrid fluorides—$(TMA)_2BF_6$:Mn^{4+} phosphors (where TMA stands for tetramethylammonium and B = Sn or Hf) with short ESLs ($\tau \leq 3.7$ ms)—have been discovered and synthesized successfully, confirming the reliability of the proposed ML strategy. Benefiting from both the structure characteristic of highly isolated $[BF_6]^{2-}$ octahedrons and the heavy Mn^{4+} doping amount, their quantum efficiencies (IQEs > 92%, EQEs > 55%; specifically, EQE = 58.1% for $(TMA)_2SnF_6$:Mn^{4+}) are almost comparable to that of the commercial KSF. Finally, based on the $(TMA)_2SnF_6$:Mn^{4+}, a high-efficiency homemade white Mini-LED backlight module with wide color gamut was fabricated as the flat-panel light source to demonstrate their potential in high-quality Mini-LED displays. This work not only brings promising Mn^{4+}-equivalent-doped fluorides with short ESLs to the sight of the phosphor community but also can be a useful reference for the future application of ML to the development of luminescent materials.

The overall process of discovering new Mn^{4+}-doped fluoride red phosphors with short ESLs using the ML strategy was organized into the following six steps (Figure 1):

(I) Collecting data of structural features and the corresponding ESLs from literature (mainly) or one's own experiments (supplementary) to build the ML dataset;

(II) Selecting the Random Forest (RF) model, an ensemble ML method (Supporting Information), to train the dataset and construct the RF model that can predict the ESL of Mn^{4+} in fluorides;

(III) Clarifying the "structure−property" relationship, i.e., the correlations between the structure and ESL, through the RF model;

(IV) Searching for unexplored host compounds according to the revealed "structure−lifetime" correlations;

(V) Using the RF model to predict the ESL of Mn^{4+} in the screened potential hosts; and

(VI) Synthesizing the Mn^{4+}-doped target phosphors experimentally, characterizing their ESLs, and comparing them with the predicted value from the RF model.

If the measured ESL value significantly differs from that predicted by the RF model, then the initial dataset must be

https://doi.org/10.1021/acsmaterialslett.4c00263
ACS Materials Lett. 2024, 6, 1790−1800

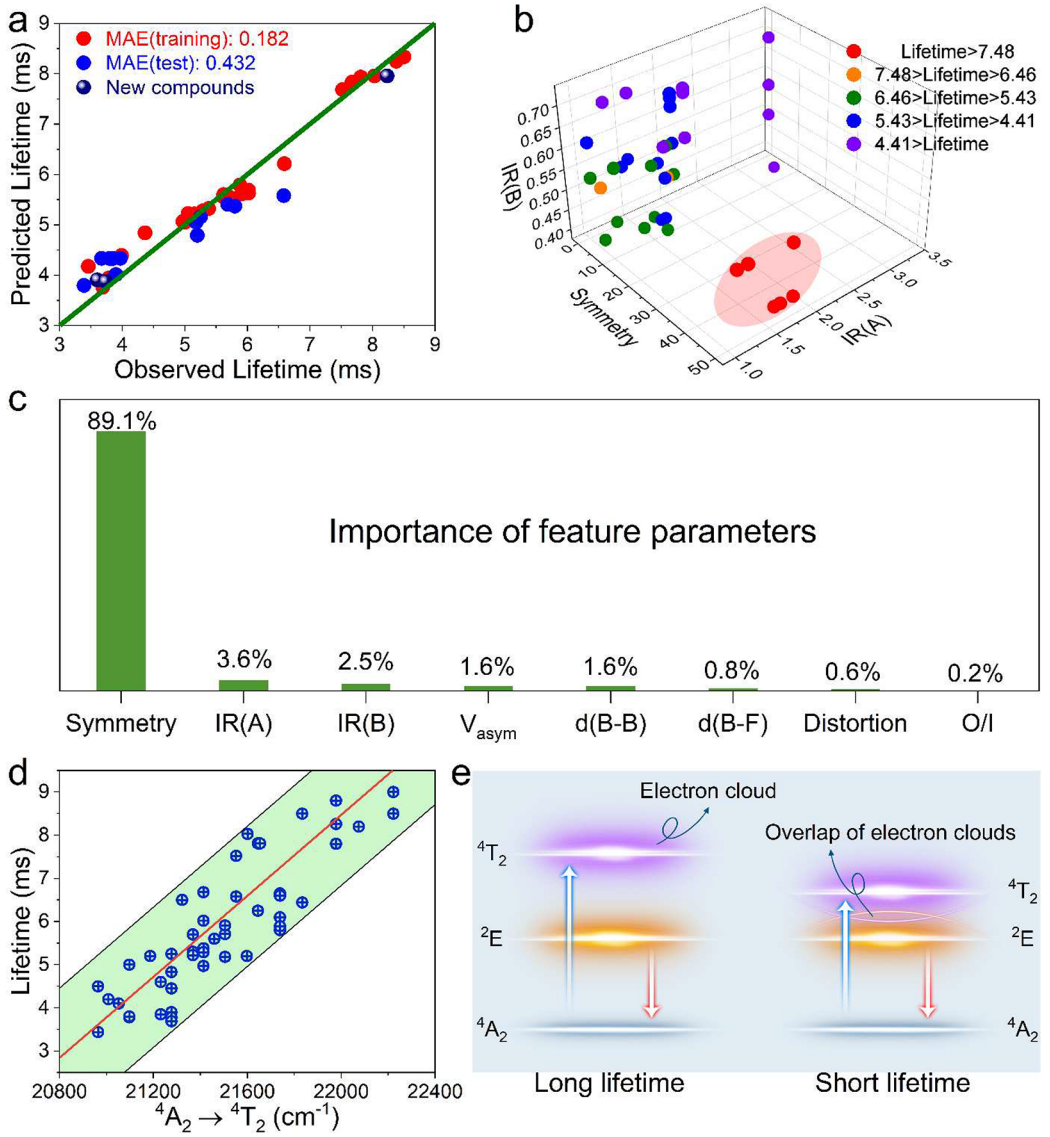

Figure 2. (a) Comparative plot of observed "Lifetime" values per predicted "Lifetime" obtained from the RF model; red circles are the training dataset (70% of the whole dataset), and blue circles are the test dataset (30% of the whole dataset). Linear fit proves the correctness of the model. Green line depicts the ideal place for circles from both datasets. Navy blue balls marked the new compounds under experimental investigation. (b) The case samples with high "Lifetime" values (red circles in the highlighted area) are segregated from others in the 3D space spanned on the three most important feature parameters. (c) Importance of all feature parameters on "Lifetime" values in the RF model. The "*Symmetry*" has the greatest influence, compared to all others. (d) ESL of Mn^{4+}-doped fluoride phosphors as a function of the $^4A_2 \rightarrow {}^4T_2$ transition energy. The red line is a linear fit of the data points. (e) Schematic energy level diagrams of Mn^{4+}-activated systems with long and short ESLs, respectively.

enhanced to further improve the RF model, until the target phosphor material is successfully obtained.

In order to obtain a reliable RF model that can predict the ESLs of Mn^{4+}-doped fluoride A_xBF_y (A = alkali metal, alkaline-earth metal, or organic ammonium cations; B = bivalent, trivalent, tetravalent, pentavalent, or hexavalent cations such as Zn^{2+}, Al^{3+}, Si^{4+}, Ge^{4+}, Nb^{5+}, and Mo^{6+}; x = 1, 2, or 3; y = 6 or 7) phosphors, we collected 65 cases of Mn^{4+}-doped fluoride red phosphors from published articles as the original ML dataset, encompassing their structural information and ESLs. More cases were added into the dataset by experiments, including hexagonal-phase KSF (Figure S1) and organic−inorganic hybrid fluoride $(TMA)_2SiF_6$:Mn^{4+} (Figure S2 and Table S1) phosphors. Additionally, the crystal structures of two all-inorganic fluorides, Rb_2TiF_6 and Cs_2TiF_6, were resolved through single-crystal X-ray diffraction (SCXRD) (Table S1), aiming to complement the missing structure features for Rb_2TiF_6:Mn^{4+} and Cs_2TiF_6:Mn^{4+} cases in the original dataset. Their crystallographic data, as well as that of $(TMA)_2SiF_6$, is deposited in the Cambridge Crystallographic Data Centre (CSD No. 2315758 for Rb_2TiF_6, CSD No. 2315760 for Cs_2TiF_6, and CCDC No. 2315757 for $(TMA)_2SiF_6$). Due to differences in synthesis methods and measurement conditions of Mn^{4+}-doped fluoride phosphors, the original dataset was rigorously screened into 40 cases, consisting of 36 all-inorganic compounds and 4 organic−inorganic hybrid compounds (Table S2), adhering to the following principles:

(1) To eliminate the influence of temperature-induced electron−phonon coupling on the ESL, only the cases

https://doi.org/10.1021/acsmaterialslett.4c00263
ACS Materials Lett. 2024, 6, 1790−1800

whose ESL measured at room temperature were retained; and

(2) To exclude poor experimental synthesis and ensure the efficient photoluminescence of phosphors as much as possible, only cases with luminescence decay curves strictly conforming to single-exponential decay characteristics were retained.

In addition, some cases (Table S2) may have several ESL values from different sources, and their average value (Table S3) was used for the ML process.

The electronic transitions of Mn^{4+} are heavily affected by the crystal field environment provided by the host matrix.[5] Consequently, to better predict the target property, i.e., the ESL, we selected seven structural parameters that are highly correlated to the Mn^{4+} local environment for feature construction of the dataset: "*IR(A)*", "*IR(B)*", "*Symmetry*", "*d(B−F)*", "*d(B−B)*", "*Distortion*", and "V_{asym}". Detailed definitions of these parameters are listed as follows:

"*IR(A)*": the ion radii of A cations in general formula A_xBF_y;

"*IR(B)*": the ion radii of B cations in the general formula A_xBF_y;

"*Symmetry*": the symmetry order of the local symmetry of the B cation in the lattice;

"*d(B−F)*": the average values of B−F bond lengths from the first coordination sphere of the B ion;

"*d(B−B)*": the average values of B−B bond lengths from the first coordination sphere of B ion;

"*Distortion*": the distortions of isolated $[BF_y]$ polyhedrons as calculated by the formula (see the Supporting Information); and

"V_{asym}": the cell volume of the asymmetric part of the unit cell.

In addition, a feature classification parameter "O/I" was added to exclude the influence of compound type, where 0 represents inorganic compound and 1 represents organic−inorganic hybrid compound. Finally, the constructed dataset of Mn^{4+}-doped fluoride phosphors for ML is listed in Table S3. The statistical plots of the dataset are summarized in Figure S3. Preliminary data analysis shows that the ESL values of phosphors (i.e., cases) are almost uniformly distributed (Figure S3), which means that all of the representative compounds were selected.

RF is an ensemble learning method based on decision trees for classification, regression, and other tasks, which is known as one of the most accurate algorithms, since a large number of trees give a more robust model.[9] Importantly, RF can be used to rank the importance of features (Figure S4), which is a very important tool for analyzing and revealing the "structure−property" relationship.[16] Therefore, the RF was used to build the ML model capable of accurately predicting the ESLs of Mn^{4+} in fluorides, namely, the RF model. The RF model was constructed by a simple self-written Python script named RandomForest.py (see the Supporting Information) using the Python 3.6 programming language.[17] The standard libraries, including numpy, pandas, sklearn, matplotlib, and mpl_toolkits, were used in the program. Due to the stochastic nature of the RF algorithm, we used its average performance across 10 repetitions of cross-validation during modeling. Each time, the dataset was divided into two random sub-datasets: one for the training process (70% of total data), and another for testing (30% of total data). The obtained mean absolute errors (MAEs) of ESL for the training set and the test set were 0.182 and 0.432 ms, respectively (Figure 2a). In addition, we have performed a 5-fold cross-validation test on the entire dataset, showing a result of MAE = 0.509 ± 0.185 ms, which is less than ∼10% of the average value (5.45 ms) of all case ESLs. The precision of prediction can be further improved by increasing the quantity of observation data, that is, the number of phosphor cases. The predicted ESL values of all cases are given in Table S4, and their differences with the observed ones are <0.4 ms for more than 75% of cases (Table S4 and Figure S5), and their overall good fit can be checked in Figure 2a. These results demonstrate the success of obtaining a reliable RF model that can predict the ESL of Mn^{4+} in fluorides.

To analyze and reveal the "structure−lifetime" correlations between the fluoride matrix and Mn^{4+}, the importance of each feature was extracted from the RF model. Feature importance refers to how much a feature contributes to prediction and is obtained based on an algorithm called "permutation importance" (Figure S4). Its fundamental idea is to shuffle a column of data while keeping the data in other columns unchanged, then observe how much the predicted metric or loss changes, and determine the feature importance on the basis of the amount of variation.[18] As shown in Figure 2c, "*Symmetry*" has the major influence (contribution up to 89.1%) on lifetime among all features, followed by "*IR(A)*", "*IR(B)*", and so on. The "*O/I*" feature contributes only 0.2% to the prediction of this RF model, indicating that the compound type has no impact on the prediction of the RF model. All cases were plotted in a 3D space of these three most important features (Figure 2b), and it can be seen that cases with long ESL and those with short ESL are clustered into a small area, respectively, showing a good separation between them. The main structural features of Mn^{4+}-doped fluoride phosphors with long (or short) ESLs can be clearly understood through the 2D plot mapped by the 3D space (Figure S6). The main rules to obtain Mn^{4+}-doped fluoride phosphors with long ESLs are as follows: (1) the symmetry order of point group of B-site local symmetry should be greater than 45; (2) the size of A-site cations should be small and less than 2.0 Å; and (3) the ionic radii of B-site cations can be in the range of 0.4−0.6 Å. The major rules for Mn^{4+}-doped fluoride phosphors with short ESLs are given as follows: (1) the symmetry order of point group of B-site local symmetry should be less than 15; (2) the ionic radii of A-site cations should preferably be greater than 3.0 Å; and (3) there is no obvious rule for the size of B-site cations. The resulting rules should be applicable to compounds with the chemical formula A_xBF_y, which means that it covers a relatively broad range of fluorides. Besides, this simple ML approach can help to reveal "structure−property" relationships for other functional materials.

Despite the main rules (i.e., the "structure−lifetime" correlations) of long (or short) ESL obtained from the ML, it is still necessary to understand the hidden physical mechanism by which structural parameters affect the electronic transition of Mn^{4+}, which can help to reasonably design new Mn^{4+}-activated phosphors with desirable luminescent properties. Based on the above ML results (Figure 2c), the "Symmetry" feature has the highest prediction contribution (up to 89.1%) to this RF model, indicating that B-site symmetry is a key structural parameter that affects the ESL. In other words, the ESL can be regulated to the greatest extent by adjusting the B-site (occupation site of Mn^{4+}) symmetry in the crystal lattice. The other six structural features also have an impact on the Mn^{4+} ESL (10.7% of the total contribution). Due to the complex 3D structure of the host matrix, there may even be undiscovered structural parameters that also influence the Mn^{4+} ESL, because this RF model temporarily cannot achieve perfect prediction for the ESL.

https://doi.org/10.1021/acsmaterialslett.4c00263
ACS Materials Lett. 2024, 6, 1790−1800

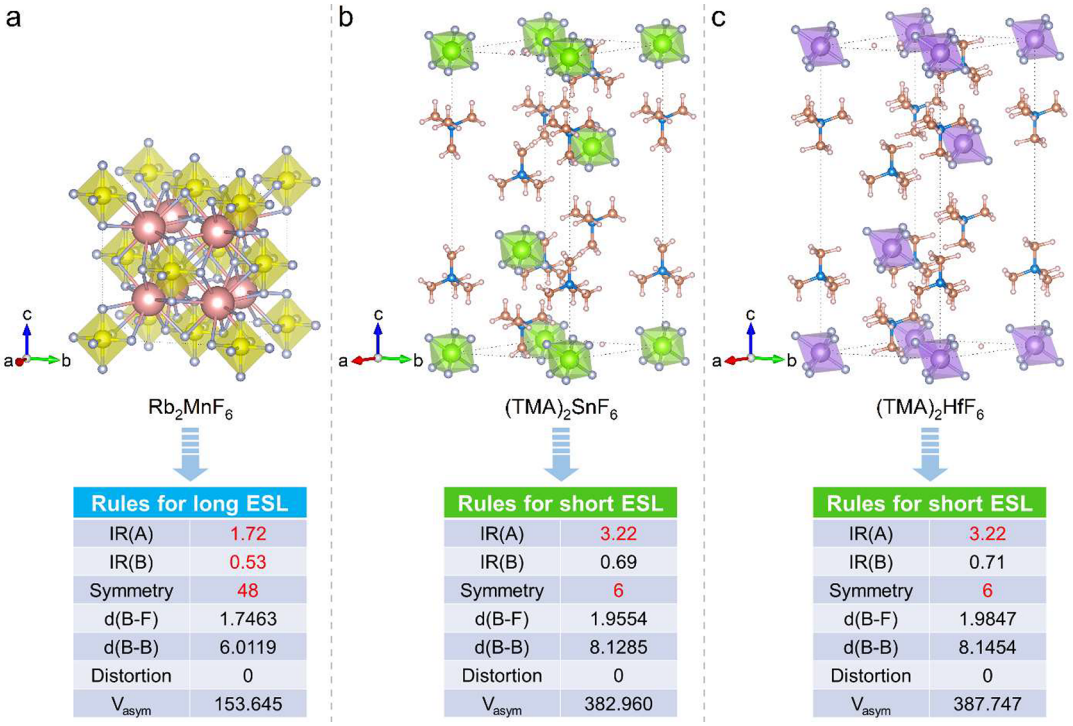

Rules for long ESL	
IR(A)	1.72
IR(B)	0.53
Symmetry	48
d(B-F)	1.7463
d(B-B)	6.0119
Distortion	0
V_{asym}	153.645

Rules for short ESL	
IR(A)	3.22
IR(B)	0.69
Symmetry	6
d(B-F)	1.9554
d(B-B)	8.1285
Distortion	0
V_{asym}	382.960

Rules for short ESL	
IR(A)	3.22
IR(B)	0.71
Symmetry	6
d(B-F)	1.9847
d(B-B)	8.1454
Distortion	0
V_{asym}	387.747

Figure 3. Crystal structures of (a) Rb_2MnF_6, (b) $(TMA)_2SnF_6$, and (c) $(TMA)_2HfF_6$, obtained from SCXRD and the structural parameters extracted from them, respectively.

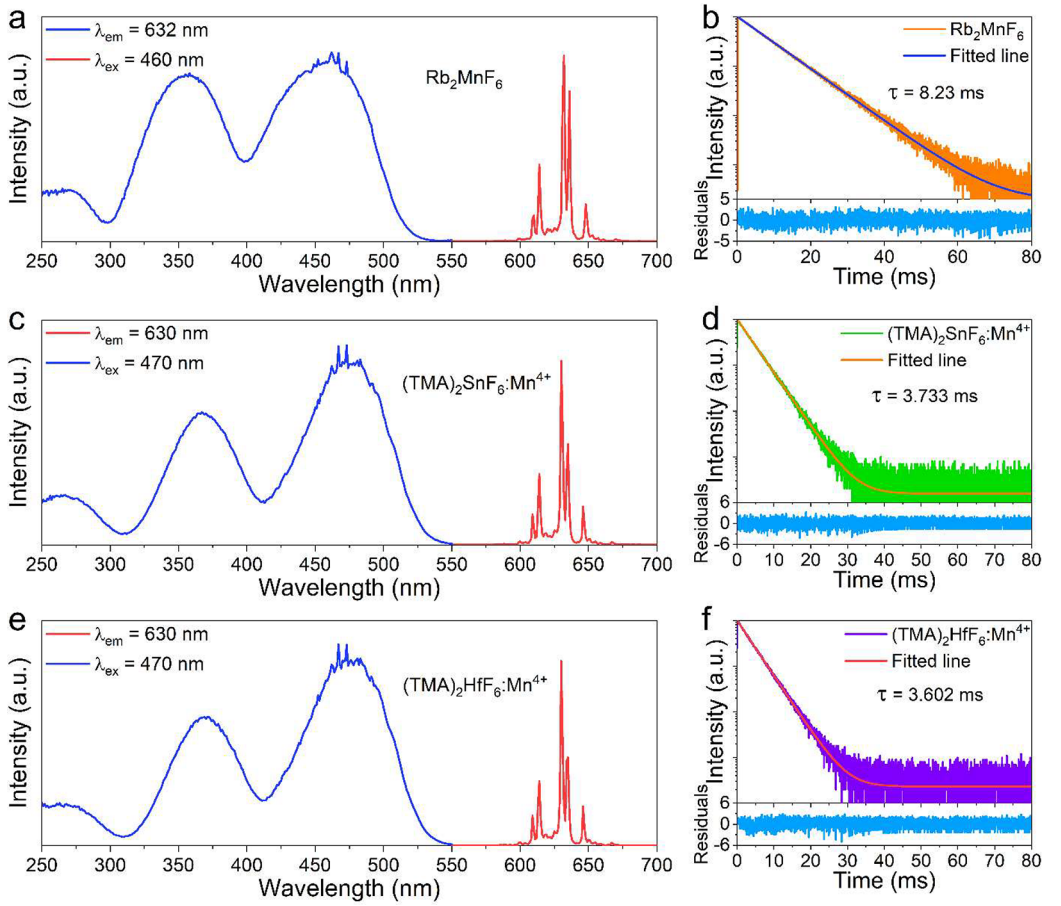

Figure 4. PLE and PL spectra, and PL decay curves of (a, b) Rb_2MnF_6, (c, d) $(TMA)_2SnF_6:Mn^{4+}$, and (e, f) $(TMA)_2HfF_6:Mn^{4+}$ measured at room temperature.

https://doi.org/10.1021/acsmaterialslett.4c00263
ACS Materials Lett. 2024, 6, 1790−1800

However, it should be emphasized that we have obtained an RF model (Figure 2a) that can well predict the Mn^{4+} ESL using only seven structural parameters; that is to say, they are responsible for the "structure−lifetime" correlations. They dominate the local crystal field environment of Mn^{4+}, thereby affecting the electronic transition of Mn^{4+}. To clarify this point, we plotted the ESL versus the $^4A_2 \rightarrow {}^4T_2$ energy for many reported Mn^{4+}-doped fluoride phosphors (Figure 2d, and data are also listed in Table S5). These data show an interesting trend where the ESL becomes shorter as the $^4T_2$ energy decreases. This obvious trend indicates that these structural parameters, especially the B-site symmetry, actually affect the $^4T_2$ energy of the incorporated Mn^{4+}, thus causing the shortening or lengthening of the ESL. A proposed energy diagram for elucidating the mechanism of ESL is drafted in Figure 2e featuring the difference of $^4T_2$ energy in the long and short ESL systems, respectively. It can be seen that the overlapping of the electron clouds of $^4T_2$ and ^2E becomes larger as the energy gap decreases, allowing more mixing in the wave functions (electron clouds) of the two energy levels, which further relaxes the spin-forbidden selection rule, resulting in a shortened ESL; conversely, the ESL will be longer. In general, these structural parameters greatly affect the relaxation of the spin-forbidden selection rule, thereby resulting in changes in the Mn^{4+} ESL.

To demonstrate the reliability of the constructed RF model and the correctness of the revealed "structure−lifetime" correlations, phosphor matrix candidates were searched from the Inorganic Crystal Structure Database (ICSD) or the CCDC. Based on the revealed structure rules of long (or short) ESL, an inorganic compound Rb_2MnF_6 was selected as the candidate for long ESL, and the other two novel tetramethylammonium (TMA)-based organic−inorganic hybrid compounds $(TMA)_2SnF_6$ and $(TMA)_2HfF_6$ as the candidates for short ESL. Their crystal structures were obtained by SCXRD analysis, as shown in Figure 3. Their main crystal data are shown in Table S6, and their crystallographic data have been deposited with the CCDC (CSD No. 2315756 for Rb_2MnF_6, CCDC No. 2315759 for $(TMA)_2SnF_6$, and CCDC No. 2315761 for $(TMA)_2HfF_6$). In addition, it can be seen that the inorganic $[BF_6]$ groups in the two hybrid structures are highly separated (d(B−B) > 8.1 Å) thanks to the steric hindrance effect of large-sized organic cations, which is beneficial to the heavy doping of Mn^{4+} while avoiding the agglomeration of Mn^{4+} and suppressing the energy transfer of Mn^{4+}−Mn^{4+} and Mn^{4+} to defects. Therefore, it can be expected that these two Mn^{4+}-doped hybrid fluorides will both have a high luminescence efficiency. In order to confirm whether these candidates possess the expected ESLs, we extracted the following structural parameters from their Crystallographic Information Files (CIFs): "*IR(A)*", "*IR(B)*", "*Symmetry*", "*d(B−F)*", "*d(B−B)*", "*Distortion*", and "V_{asym}" (see Figure 3 and Table S3). These structural parameters and the classification feature "*O/I*" were uploaded to the constructed RF model, and the predicted ESL values of Mn^{4+} in these compounds were obtained using the conventional procedure of averaging the Forest voting: 7.958, 3.877, and 3.908 ms for Rb_2MnF_6, $(TMA)_2SnF_6$:Mn^{4+}, and $(TMA)_2HfF_6$:Mn^{4+}, respectively (see Table S4 and Figure 2a). To verify the accuracy of this RF model prediction, we carried out experimental confirmation (see the Supporting Information), where Rb_2MnF_6 was directly used for characterization since it is a Mn^{4+}-base compound crystal (Figure S7). XRD analysis (Figure S8) showed that a series of pure $(TMA)_2BF_6$:Mn^{4+} (B = Sn or Hf) phosphor samples doped with various Mn^{4+} concentrations (Table S7) were synthesized successfully. Rb_2MnF_6 and $(TMA)_2BF_6$:Mn^{4+} (B = Sn or Hf) both exhibit typical luminescence characteristics of Mn^{4+} in fluorides (Figure 4), where the concentration-dependent PL spectra of $(TMA)_2BF_6$:Mn^{4+} indicate that their optimal doping amounts of Mn^{4+} are ∼20% (Figure S9). The IQEs (92.0% and 94.4%) and EQEs (58.1% and 55.4%) of $(TMA)_2BF_6$:20 mol % Mn^{4+} have exceeded those of most reported Mn^{4+}-activated fluoride red phosphors, and are almost comparable to that of commercial KSF with long ESL (Table 1). Their high QEs can be ascribed to the structure characteristics of highly isolated $[BF_6]^{2-}$ octahedrons and the heavy Mn^{4+} doping amount. The Rb_2MnF_6 crystal phosphor also shows high IQE and EQE of 81.4% and 63.5%, respectively. Its high QEs result from the 100% Mn^{4+} content and the large single crystal particles. In the meantime, their luminescence decay curves all showed single-exponential decay behavior (Figure 4), which means that the PL decay starting from the ^2E excited state is mainly radiative, confirming they have excellent photoluminescence performances. Their actual measured ESLs were 8.23 ms (Rb_2MnF_6), 3.733 ms ($(TMA)_2SnF_6$:Mn^{4+}), and 3.602 ms ($(TMA)_2HfF_6$:Mn^{4+}), respectively; and their differences from

Table 1. IQE, AE, EQE, and Corresponding Excited-State Lifetime (ESL) of Some Typical Mn^{4+}-Doped Fluoride Phosphors[a]

phosphor	IQE (%)	AE (%)	EQE (%)	ESL (ms)	ref
K_2SiF_6:Mn^{4+}	90.4	86.5	78.2	7.6	8
K_2SiF_6:Mn^{4+}	93.3	72.3	67.5	8.1	8
K_2SiF_6:Mn^{4+}	92	47.8	44	8.3	19
$KNaSiF_6$:Mn^{4+}	90	45.5	41	6.1	20
Rb_2SiF_6:Mn^{4+}	91.9	60.7	55.8	8.01	21
Cs_2SiF_6:Mn^{4+}	89.22	79.96	71.34	7.81	22
Na_2GeF_6:Mn^{4+}	60	/	/	6.58	23
K_2GeF_6:Mn^{4+}	93	78	73	6.65	24
K_2GeF_6:Mn^{4+}	97.9	70.3	68.8	6.6	25
K_2GeF_6:Mn^{4+}	90	66.6	60	5.85	26
Cs_2GeF_6:Mn^{4+}	80	83.7	66.9	7.52	23, 27
K_2TiF_6:Mn^{4+}	93	54	50.22	5.7	1
K_2TiF_6:Mn^{4+}	94	69	64.86	6.35	28
K_2TiF_6:Mn^{4+}@ K_2TiF_6	96	69	66.24	6.25	28
Rb_2TiF_6:Mn^{4+}	76	/	/	5.2	29
Rb_2ZrF_6:Mn^{4+}	75	/	/	5.0	30
Rb_2SnF_6:Mn^{4+}	70.3	/	/	5.22	31
K_3AlF_6:Mn^{4+}	88	57.5	50.6	5.2	32
K_2NaAlF_6:Mn^{4+}	58.4	/	/	7.537	33
K_2NaAlF_6:Mn^{4+}	88	17	14.96	7.81	34
Na_3GaF_6:Mn^{4+}	69	/	/	4.97	35
K_2NbF_7:Mn^{4+}	93.5	28.0	26.2	3.7	6
K_2NaScF_6:Mn^{4+}	70.3	18.2	12.8	3.5	36
K_3GaF_6:Mn^{4+}	46	/	/	3.69	37
K_2LiAlF_6:Mn^{4+}	87.5	17.9	15.7	9.3	38
K_2NaAlF_6:Mn^{4+}	85	26	22.1	7.58	34
K_2NaGaF_6:Mn^{4+}	61	/	/	5.6	39
K_2NaScF_6:Mn^{4+}	57.13	15.91	9.09	1.78	5
Rb_2NaScF_6:Mn^{4+}	54.98	18.88	10.38	3.69	5
Cs_2NaScF_6:Mn^{4+}	51.99	20.81	10.82	3.31	5
Rb_2MnF_6	81.4	78.0	63.5	8.23	this work
$(TMA)_2SnF_6$:Mn^{4+}	92.0	63.1	58.1	3.733	this work
$(TMA)_2HfF_6$:Mn^{4+}	94.4	58.7	55.4	3.602	this work

[a]Note: "/" denotes no reference data.

https://doi.org/10.1021/acsmaterialslett.4c00263
ACS Materials Lett. 2024, 6, 1790−1800

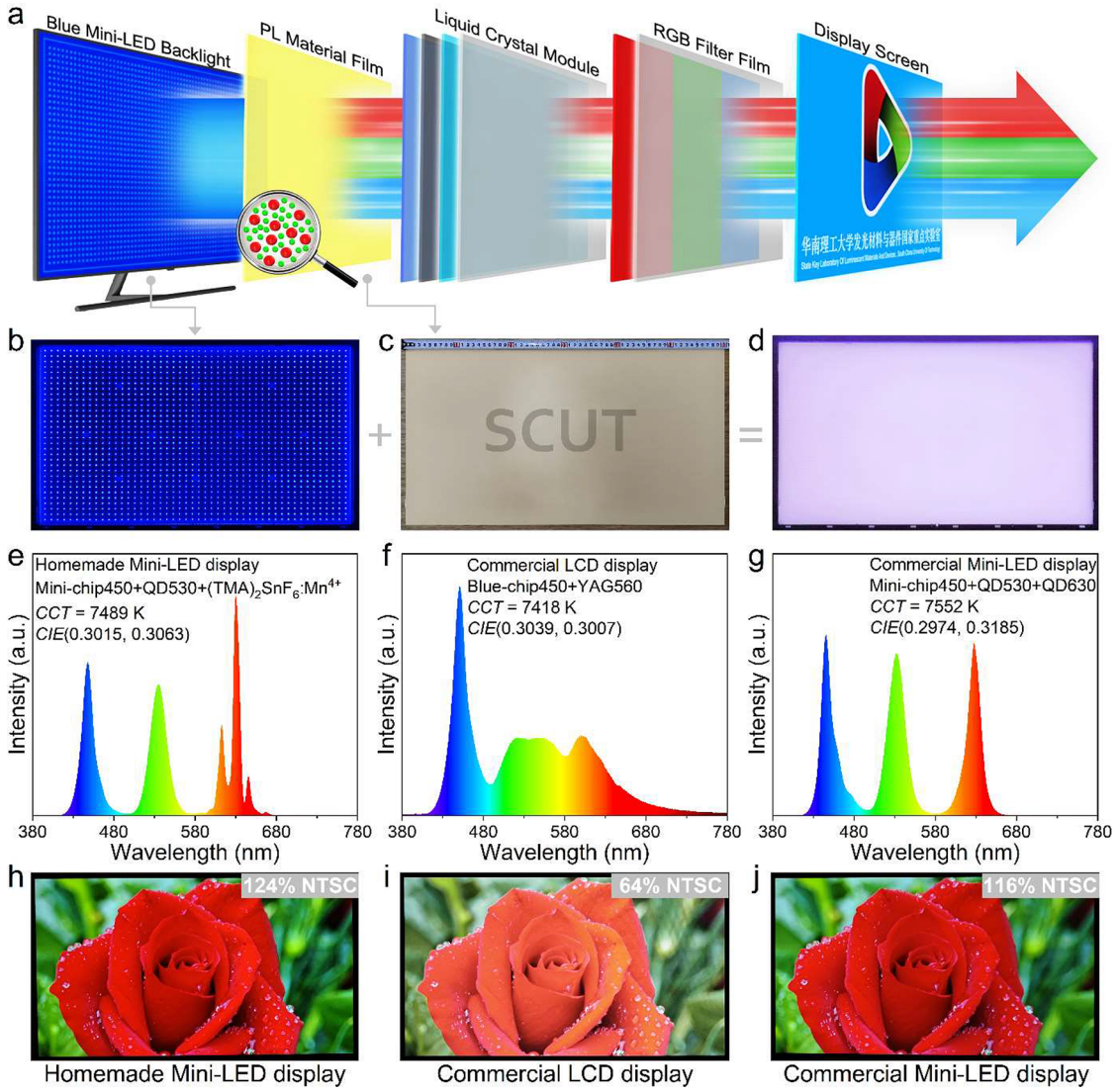

Figure 5. (a) Schematic diagram of the homemade mini-LED display prototype in this work. (b) Photograph of the internal blue mini-LED backlight for the display prototype when powered on. (c) Photograph of the PL material film coated by a mixture of $(TMA)_2SnF_6:Mn^{4+}$ and green QD (~530 nm) taken under natural light. (d) Photograph of the white backlight module assembled by directly placing the PL material film on the surface of the blue mini-LED backlight when powered on. Output spectra were collected from the screens of the homemade mini-LED display prototype (panel) (e)), a YAG phosphor-based commercial LCD display (panel (f)), and a QD-based commercial mini-LED display (panel (g)), using a fiber optic spectrometer. Comparison of the images displayed by the homemade mini-LED display prototype (panel (h)), the YAG phosphor-based commercial LCD display (panel (i)), and the QD-based commercial mini-LED display (panel (j)).

the RF model predicted values were 0.272 ms (Rb_2MnF_6), −0.144 ms ($(TMA)_2SnF_6:Mn^{4+}$), and −0.306 ms ($(TMA)_2HfF_6:Mn^{4+}$), respectively (Table S4). All the differences were below the obtained MAE value (0.509 ± 0.185 ms), demonstrating the good prediction credibility of the RF model and the correctness of the revealed "structure−lifetime" correlations. Therefore, the constructed RF model can be used to screen unexplored compounds to find new Mn^{4+}-doped phosphor candidates with long/short ESLs and allow researchers to select the desired materials before proceeding with conventional synthesis procedure. And more notably, unlike those previously reported Mn^{4+}-doped fluoride phosphors, the discovered $(TMA)_2BF_6:Mn^{4+}$ phosphors simultaneously achieve high QEs and short ESLs (Table 1). In addition, the short ESLs of $(TMA)_2BF_6:Mn^{4+}$ can greatly suppress the red luminescence tailing phenomenon, as illustrated in Figure S10, which is beneficial for fast-response backlight displays.[5]

Evidently, temperature-dependence experiments (Figure S11) indicate that the $(TMA)_2BF_6:Mn^{4+}$ phosphors are not suitable for high-power pc-WLED applications, because their red emission is severely quenched at 150 °C (423 K).[4] This quenching phenomenon is due to their relatively "soft" 0D crystal structure, which lacks structural rigidity compared with the KSF. Fortunately, the vast majority of their red emission can be preserved at 75 °C (e.g., 84.2% for $(TMA)_2SnF_6:Mn^{4+}$), which is higher than the LED junction temperature (merely 70 °C) in backlight displays.[6]

The high QEs, short ESLs, bearable thermal quenching, wide blue absorption, and narrow red emission make $(TMA)_2BF_6:Mn^{4+}$ a promising emitter for high-quality wide color gamut mini-LED backlight displays. Based on the internal layout of the mini-LED display (Figure 5a), we first need to prepare a PL material film with appropriate light transmittance that can be completely covered on the blue mini-LED backlight

https://doi.org/10.1021/acsmaterialslett.4c00263
ACS Materials Lett. 2024, 6, 1790−1800

(Figure 5b) to assemble a white backlight module. The small size of $(TMA)_2BF_6:Mn^{4+}$ helps them to be coated into a uniform film (Figure S12). The PL material film was coated by a homogeneous mixture of the $(TMA)_2SnF_6:Mn^{4+}$, commercial quantum dot (QD530) and isobornyl acrylate through a wire rod coating machine. As the photographs show in Figure 5c, the as-prepared yellow PL material film is uniform and translucent and was cut to dimensions similar to that of a 27 in. monitor screen. Then, this film was placed on the blue mini-LED backlight to assemble the white backlight module (Figure S13). A strong white light emission can be observed from it when powered on (Figure 5d). Moreover, due to the small heat generation of the mini blue chips and the noncontact design between the film and the chips, the maximum working temperature of the PL material film on the white backlight module is 31.4 °C (Figure S13), which is far lower than the thermal quenching temperature of these $(TMA)_2BF_6:Mn^{4+}$ phosphors ($T_{1/2}$ = 116 or 109 °C, Figure S11). In addition, due to the protection of the film by the polyethylene terephthalate (PET) substrates, no significant decrease in luminescent intensity was observed when the white backlight module was continuously lit in a 65% high-humidity environment for 48 h (Figure S14), indicating good stability of the module. According to the configuration of the mini-LED display mentioned above, this white backlight module was used with a commercial liquid crystal module, RGB filter film, and display screen to assemble a homemade mini-LED display prototype to demonstrate the display performance. The homemade prototype display screen emits standard cool white light with a correlated color temperature (CCT) of 7489 K and Commission Internationale de L'Eclairage (CIE) chromaticity coordinates of (0.3015, 0.3063), which is similar to the white light emitted by the commercial $Y_3Al_5O_{12}:Ce^{3+}$ (YAG) phosphor-based liquid crystal display (LCD) (CCT = 7418 K, CIE = (0.3039, 0.3007)) and QD-based mini-LED display (CCT = 7552 K, CIE = (0.2974, 0.3185)) (Figures 5e–g). Based on the filtered pure red, green, and blue spectra of this homemade prototype display (Figure S15), its color gamut was determined to be ∼124% of the National Television Standards Committee (NTSC) standard in the CIE 1931 color space, which is much higher than the commercial LCD display with broad emission spectral characteristics (64% NTSC, Figure S16). Furthermore, due to the narrower red emission of $(TMA)_2SnF_6:Mn^{4+}$ compared to commercial QD630 (Figure S17), its color gamut is also larger than that of the QD-based commercial mini-LED display (116% NTSC, Figure S18). Thanks to the wider color gamut brought by the homemade white backlight module, the $(TMA)_2SnF_6:Mn^{4+}$-based homemade Mini-LED display prototype exhibits a more vivid picture of the red rose compared to the other two commercial displays (Figures 5h–j). In addition, since it is impossible to measure the luminous efficiency (LE) of the large-size display devices, we also fabricated two conventional pc-WLEDs with standard white light emission based on the $(TMA)_2SnF_6:Mn^{4+}$ phosphors (Figure S19). They all exhibit high LEs (122.42 or 135.99 lm/W), showing great practical prospects of the $(TMA)_2SnF_6:Mn^{4+}$ phosphors in backlight displays. These results show that we have taken a substantial advance toward the commercial application of high-quality mini-LED displays with the help of $(TMA)_2BF_6:Mn^{4+}$ phosphors.

In conclusion, we have demonstrated an efficient ML approach based on a relatively small dataset to discover new Mn^{4+}-doped fluoride red phosphors with desired ESLs. Such a ML approach not only builds an RF model that can accurately predict the ESLs of Mn^{4+} in fluorides, but also elucidates the "structure–lifetime" correlations between the fluoride matrix and Mn^{4+}. Feature importance results indicate that the B-site symmetry is a pivotal structural feature that determines the ESL of Mn^{4+}. The underlying mechanism lies in the interesting intertwinements between these structural parameters (especially the B-site symmetry) and the $^4T_2$ energy of Mn^{4+} that affects the ESLs by controlling the mixing of $^4T_2$ and ^2E wave functions. Under the guidance of "structure–lifetime" correlations and the RF model prediction, short ESLs ($\tau \leq 3.7$ ms) were achieved in two new Mn^{4+}-doped fluoride $(TMA)_2BF_6:Mn^{4+}$ (B = Sn or Hf) phosphors, respectively. Their EQEs are comparable to that of the commercial KSF (e.g., EQE = 58.1% for $(TMA)_2SnF_6:Mn^{4+}$), but their ESLs are less than half that of KSF. Employing $(TMA)_2SnF_6:Mn^{4+}$, the prototype display with excellent performance (∼124% NTSC) was assembled based on the homemade white mini-LED backlight module, demonstrating the practical prospects of $(TMA)_2BF_6:Mn^{4+}$ phosphors in high-quality displays. This work provides a deeper understanding on the correlations between structure and luminescence, as well as lays the groundwork for future advancement in employing ML to dramatically accelerate the discovery of new promising phosphors.

■ ASSOCIATED CONTENT

Supporting Information

The Supporting Information is available free of charge at https://pubs.acs.org/doi/10.1021/acsmaterialslett.4c00263.

Cambridge Crystallographic Data Centre data for Cs_2TiF_6 (CSD No. 2315760) (CIF)

Cambridge Crystallographic Data Centre data for Rb_2MnF_6 (CSD No. 2315756) (CIF)

Cambridge Crystallographic Data Centre data for Rb_2TiF_6 (CSD No. 2315758) (CIF)

Cambridge Crystallographic Data Centre data for $(TMA)_2SnF_6$ (CSD No. 2315759) (CIF)

Cambridge Crystallographic Data Centre data for $(TMA)_2SiF_6$ (CSD No. 2315757) (CIF)

Cambridge Crystallographic Data Centre data for $(TMA)_2HfF_6$ (CSD No. 2315761) (CIF)

Experimental details, ML method, supplementary text, and supporting figures and tables, including XRD, photoluminescence excitation (PLE), PL, ESL, scanning electron microscopy (SEM), device performance and photographs, main crystal structural parameters for selected compounds, collected cases for the ML, and inductively coupled plasma–optical emission spectrometry (ICP-OES) results (PDF)

Accession Codes

CCDC or CSD Nos. 2315756–2315761 contain the supplementary crystallographic data for this paper. These data can be obtained free of charge from the Cambridge Crystallographic Data Centre via www.ccdc.cam.ac.uk/data_request/cif.

■ AUTHOR INFORMATION

Corresponding Authors

Enhai Song − *State Key Laboratory of Luminescent Materials and Devices, Guangdong Provincial Key Laboratory of Fiber Laser Materials and Applied Techniques, and Guangdong Engineering Technology Research and Development Center of Special Optical Fiber Materials and Devices, South China*

https://doi.org/10.1021/acsmaterialslett.4c00263
ACS Materials Lett. 2024, 6, 1790−1800

University of Technology, Guangzhou 510641, China; School of Materials Science and Engineering, South China University of Technology, Guangzhou 510641, China; orcid.org/0000-0003-1666-0532; Email: msehsong@scut.edu.cn

Yayun Zhou − *State Key Laboratory of Luminescent Materials and Devices, Guangdong Provincial Key Laboratory of Fiber Laser Materials and Applied Techniques, and Guangdong Engineering Technology Research and Development Center of Special Optical Fiber Materials and Devices, South China University of Technology, Guangzhou 510641, China; School of Materials Science and Engineering, South China University of Technology, Guangzhou 510641, China; Guangdong-Hong Kong-Macao Joint Laboratory for Intelligent Micro-Nano Optoelectronic Technology, School of Physics and Optoelectronic Engineering, Foshan University, Foshan 528225, China*; Email: zhouyayun@fosu.edu.cn

Qinyuan Zhang − *State Key Laboratory of Luminescent Materials and Devices, Guangdong Provincial Key Laboratory of Fiber Laser Materials and Applied Techniques, and Guangdong Engineering Technology Research and Development Center of Special Optical Fiber Materials and Devices, South China University of Technology, Guangzhou 510641, China; School of Materials Science and Engineering and School of Physics and Optoelectronics, South China University of Technology, Guangzhou 510641, China;* orcid.org/0000-0001-6544-4735; Email: qyzhang@scut.edu.cn

Authors

Hong Ming − *State Key Laboratory of Luminescent Materials and Devices, Guangdong Provincial Key Laboratory of Fiber Laser Materials and Applied Techniques, and Guangdong Engineering Technology Research and Development Center of Special Optical Fiber Materials and Devices, South China University of Technology, Guangzhou 510641, China; School of Materials Science and Engineering, South China University of Technology, Guangzhou 510641, China; International Center for Materials Nanoarchitectonics (MANA), National Institute for Materials Science (NIMS), Tsukuba 305-0047, Japan;* orcid.org/0000-0003-0118-1897

Maxim S. Molokeev − *Laboratory of Crystal Physics, Kirensky Institute of Physics, Federal Research Center KSC SB RAS, Krasnoyarsk 660036, Russia; Laboratory of Theory and Optimization of Chemical and Technological Processes, University of Tyumen, Tyumen 625003, Russia; Institute of Engineering Physics and Radioelectronics, Siberian Federal University, Krasnoyarsk 660041, Russia;* orcid.org/0000-0002-8297-0945

Chuang Zhang − *State Key Laboratory of Luminescent Materials and Devices, Guangdong Provincial Key Laboratory of Fiber Laser Materials and Applied Techniques, and Guangdong Engineering Technology Research and Development Center of Special Optical Fiber Materials and Devices, South China University of Technology, Guangzhou 510641, China; School of Physics and Optoelectronics, South China University of Technology, Guangzhou 510641, China*

Lin Huang − *Fujian Key Laboratory of Surface and Interface Engineering for High Performance Materials and College of Materials, Xiamen University, Xiamen 361005, China*

Yuanjing Wang − *State Key Laboratory of Luminescent Materials and Devices, Guangdong Provincial Key Laboratory of Fiber Laser Materials and Applied Techniques, and Guangdong Engineering Technology Research and Development Center of Special Optical Fiber Materials and Devices, South China University of Technology, Guangzhou 510641, China; School of Physics and Optoelectronics, South China University of Technology, Guangzhou 510641, China*

Hong-Tao Sun − *International Center for Materials Nanoarchitectonics (MANA), National Institute for Materials Science (NIMS), Tsukuba 305-0047, Japan*

Complete contact information is available at: https://pubs.acs.org/10.1021/acsmaterialslett.4c00263

Author Contributions

H.M., Y.Z., E. S., and Q.Z. conceived the idea and initiated the research. Q.Z. supervised the project. H.M. and M.S.M. performed the machine learning and analyzed the results. H.M., and C.Z. designed the experiments. H.M., and C.Z. performed the experiments and collected the data. H.M., Y.Z., C.Z., L.H., Y.W., E.S., H.S., and Q.Z. analyzed the data and discussed the results. Y.Z. conducted the construction of mini-LED display devices and analyzed them. H.M. wrote the manuscript, and E.S., H.S. and Q.Z. revised and commented on it. CRediT: **Hong Ming** conceptualization, investigation, software, writing-original draft, writing-review & editing; **Yayun Zhou** conceptualization, funding acquisition, supervision, writing-review & editing; **Maxim S. Molokeev** methodology, software; **Chuang Zhang** data curation, methodology, writing-original draft; **Hong-Tao Sun** data curation, writing-original draft; **Enhai Song** conceptualization, funding acquisition, supervision, writing-review & editing; **Qinyuan Zhang** conceptualization, funding acquisition, supervision, writing-review & editing.

Notes

The authors declare no competing financial interest.

■ ACKNOWLEDGMENTS

This work was financially supported by the National Key Research and Development Program of China (No. 2022YFB3503800), National Natural Science Foundation of China (Grants Nos. 52202170 and 52322208), Natural Science Foundation of Guangdong Province (No. 2022A1515140032) and Distinguished Youth Foundation of Guangdong Scientific Committee (No. 2023B1515020059). This work was also supported by the Tyumen Oblast Government, as part of the West-Siberian Interregional Science and Education Center's Project No. 89-DON (3). H. Ming acknowledges the fellowship support from the China Scholarship Council (CSC No. 202206150038).

■ REFERENCES

(1) Zhu, H.; Lin, C. C.; Luo, W.; Shu, S.; Liu, Z.; Liu, Y.; Kong, J.; Ma, E.; Cao, Y.; Liu, R. S.; Chen, X. Highly efficient non-rare-earth red emitting phosphor for warm white light-emitting diodes. *Nat. Commun.* **2014**, *5*, 4312.

(2) Senden, T.; van Dijk-Moes, R. J. A.; Meijerink, A. Quenching of the red Mn^{4+} luminescence in Mn^{4+}-doped fluoride LED phosphors. *Light Sci. Appl.* **2018**, *7*, 8.

(3) Ming, H.; Zhao, Y. F.; Zhou, Y. Y.; Molokeev, M. S.; Wang, Y. J.; Zhang, S.; Song, E. H.; Ye, S.; Xia, Z. G.; Zhang, Q. Y. Shining Mn^{4+} in 0D Organometallic Fluoride Hosts towards Highly Efficient Photoluminescence. *Adv. Opt. Mater.* **2022**, *10*, 2102141.

(4) van de Haar, M. A.; Tachikirt, M.; Berends, A. C.; Krames, M. R.; Meijerink, A.; Rabouw, F. T. Saturation Mechanisms in Common LED Phosphors. *ACS Photonics* **2021**, *8*, 1784−1793.

(5) Zhou, Y. Y.; Song, E. H.; Brik, M. G.; Wang, Y. J.; Hu, T.; Xia, Z. G.; Zhang, Q. Y. Non-equivalent Mn^{4+} doping into A_2NaScF_6 (A = K, Rb, Cs) hosts toward short fluorescence lifetime for backlight display application. *J. Mater. Chem. C* **2019**, *7*, 9203−9210.
(6) Lin, H.; Hu, T.; Huang, Q.; Cheng, Y.; Wang, B.; Xu, J.; Wang, J.; Wang, Y. Non-Rare-Earth K_2XF_7:Mn^{4+} (X = Ta, Nb): A Highly-Efficient Narrow-Band Red Phosphor Enabling the Application in Wide-Color-Gamut LCD. *Laser Photonics Rev.* **2017**, *11*, 1700148.
(7) Wang, Y.; Zhou, Y.; Ming, H.; Zhao, Y.; Song, E.; Zhang, Q. Luminescence Enhancement of Mn^{4+}-Activated Fluorides via a Heterovalent Co-Doping Strategy for Monochromatic Multiplexing. *ACS Appl. Mater. Interfaces* **2021**, *13*, 51255−51265.
(8) Zhou, Y.; Yu, C.; Song, E.; Wang, Y.; Ming, H.; Xia, Z.; Zhang, Q. Three Birds with One Stone: K_2SiF_6:Mn^{4+} Single Crystal Phosphors for High-Power and Laser-Driven Lighting. *Adv. Opt. Mater.* **2020**, *8*, 2000976.
(9) Molokeev, M. S.; Su, B.; Aleksandrovsky, A. S.; Golovnev, N. N.; Plyaskin, M. E.; Xia, Z. Machine Learning Analysis and Discovery of Zero-Dimensional ns^2 Metal Halides toward Enhanced Photoluminescence Quantum Yield. *Chem. Mater.* **2022**, *34*, 537−546.
(10) Zhuo, Y.; Mansouri Tehrani, A.; Oliynyk, A. O.; Duke, A. C.; Brgoch, J. Identifying an efficient, thermally robust inorganic phosphor host via machine learning. *Nat. Commun.* **2018**, *9*, 4377.
(11) Park, C.; Lee, J. W.; Kim, M.; Lee, B. D.; Singh, S. P.; Park, W. B.; Sohn, K. S. A data-driven approach to predicting band gap, excitation, and emission energies for Eu^{2+}-activated phosphors. *Inorg. Chem. Front.* **2021**, *8*, 4610−4624.
(12) Fang, M. H.; Wu, W. L.; Jin, Y.; Lesniewski, T.; Mahlik, S.; Grinberg, M.; Brik, M. G.; Srivastava, A. M.; Chiang, C. Y.; Zhou, W.; et al. Control of Luminescence by Tuning of Crystal Symmetry and Local Structure in Mn^{4+}-Activated Narrow Band Fluoride Phosphors. *Angew. Chem., Int. Ed. Engl.* **2018**, *57*, 1797−1801.
(13) Ming, H.; Zhao, Y.; Zhou, Y.; Molokeev, M. S.; Wang, Y.; Song, E.; Zhang, Q. Chemical Group Substitution Enables Highly Efficient Mn^{4+} Luminescence in Heterovalent Systems. *Adv. Opt. Mater.* **2023**, *11*, 2300076.
(14) Adachi, S. Photoluminescence spectra and modeling analyses of Mn^{4+}-activated fluoride phosphors: A review. *J. Lumin.* **2018**, *197*, 119−130.
(15) Jiang, L.; Jiang, X.; Wang, C.; Liu, P.; Zhang, Y.; Lv, G.; Lookman, T.; Su, Y. Rapid Discovery of Efficient Long-Wavelength Emission Garnet:Cr NIR Phosphors via Multi-Objective Optimization. *ACS Appl. Mater. Interfaces* **2022**, *14*, 52124−52133.
(16) Choe, H.; Jin, H.; Lee, S. J.; Cho, J. Machine Learning-Directed Predictive Models: Deciphering Complex Energy Transfer in Mn-Doped $CsPb(Cl_{1-y}Br_y)_3$ Perovskite Nanocrystals. *Chem. Mater.* **2023**, *35*, 5401−5411.
(17) Coelho, L. P.; Richert, W.; Brucher, M. *Building Machine Learning Systems with Python: Explore machine learning and deep learning techniques for building intelligent systems using scikit-learn and TensorFlow*; Packt Publishing Ltd., 2018.
(18) Zhu, R.; Zeng, D.; Kosorok, M. R. Reinforcement learning trees. *J. Am. Stat. Assoc.* **2015**, *110*, 1770−1784.
(19) Hou, Z. Y.; Tang, X. Y.; Luo, X. F.; Zhou, T. L.; Zhang, L.; Xie, R. J. A green synthetic route to the highly efficient K_2SiF_6:Mn^{4+} narrow-band red phosphor for warm white light-emitting diodes. *J. Mater. Chem. C* **2018**, *6*, 2741−2746.
(20) Jin, Y.; Fang, M. H.; Grinberg, M.; Mahlik, S.; Lesniewski, T.; Brik, M. G.; Luo, G. Y.; Lin, J. G.; Liu, R. S. Narrow Red Emission Band Fluoride Phosphor $KNaSiF_6$:Mn^{4+} for Warm White Light-Emitting Diodes. *ACS Appl. Mater. Interfaces* **2016**, *8*, 11194−11203.
(21) Zhou, Y.; Ming, H.; Zhao, Y.; Wang, Y.; Song, E.; Xia, Z.; Zhang, Q. Preparation and Luminescent Properties of Rb_2SiF_6:Mn^{4+} Single Crystal for Laser Lighting. *Chin. J. Lumin.* **2021**, *42*, 1559−1568.
(22) Song, E. H.; Zhou, Y. Y.; Yang, X. B.; Liao, Z. F.; Zhao, W. R.; Deng, T. T.; Wang, L. Y.; Ma, Y. Y.; Ye, S.; Zhang, Q. Y. Highly Efficient and Stable Narrow-Band Red Phosphor Cs_2SiF_6:Mn^{4+} for High-Power Warm White LED Applications. *ACS Photonics* **2017**, *4*, 2556−2565.
(23) Lian, H.; Huang, Q.; Chen, Y.; Li, K.; Liang, S.; Shang, M.; Liu, M.; Lin, J. Resonance Emission Enhancement (REE) for Narrow Band Red-Emitting A_2GeF_6:Mn^{4+} (A = Na, K, Rb, Cs) Phosphors Synthesized via a Precipitation-Cation Exchange Route. *Inorg. Chem.* **2017**, *56*, 11900−11910.
(24) Zhou, W.; Fang, M. H.; Lian, S.; Liu, R. S. Ultrafast Self-Crystallization of High-External-Quantum-Efficient Fluoride Phosphors for Warm White Light-Emitting Diodes. *ACS Appl. Mater. Interfaces* **2018**, *10*, 17508−17511.
(25) Huang, L.; Liu, Y.; Si, S.; Brik, M. G.; Wang, C.; Wang, J. A new reductive dl-mandelic acid loading approach for moisture-stable Mn^{4+} doped fluorides. *Chem. Commun.* **2018**, *54*, 11857−11860.
(26) Lang, T.; Fang, S.; Han, T.; Wang, M.; Yang, D.; Wang, J.; Cao, S.; Peng, L.; Liu, B.; Cai, M.; et al. Phase Transformation of a K_2GeF_6 Polymorph for Phosphors Driven by a Simple Precipitation-Dissolution Equilibrium and Ion Exchange. *Inorg. Chem.* **2020**, *59*, 8298−8307.
(27) Wang, Z.; Yang, Z.; Wang, N.; Zhou, Q.; Zhou, J.; Ma, L.; Wang, X.; Xu, Y.; Brik, M. G.; Dramićanin, M. D.; Wu, M. Single-Crystal Red Phosphors: Enhanced Optical Efficiency and Improved Chemical Stability for wLEDs. *Adv. Opt. Mater.* **2020**, *8*, 1901512.
(28) Huang, D.; Zhu, H.; Deng, Z.; Zou, Q.; Lu, H.; Yi, X.; Guo, W.; Lu, C.; Chen, X. Moisture-Resistant Mn^{4+}-Doped Core-Shell-Structured Fluoride Red Phosphor Exhibiting High Luminous Efficacy for Warm White Light-Emitting Diodes. *Angew. Chem., Int. Ed. Engl.* **2019**, *58*, 3843−3847.
(29) Sakurai, S.; Nakamura, T.; Adachi, S. Editors' Choice—Rb_2SiF_6:Mn^{4+} and Rb_2TiF_6:Mn^{4+} Red-Emitting Phosphors. *ECS J. Solid State Sci. Technol.* **2016**, *5*, R206−R210.
(30) Wang, L. Y.; Song, E. H.; Zhou, Y. Y.; Deng, T. T.; Ye, S.; Zhang, Q. Y. An efficient and stable narrow band Mn^{4+}-activated fluorotitanate red phosphor Rb_2TiF_6:Mn^{4+} for warm white LED applications. *J. Mater. Chem. C* **2018**, *6*, 8670−8678.
(31) Jiang, C. Y.; Brik, M. G.; Srivastava, A. M.; Li, L. H.; Peng, M. Y. Significantly conquering moisture-induced luminescence quenching of red line-emitting phosphor Rb_2SnF_6:Mn^{4+} through $H_2C_2O_4$ triggered particle surface reduction for blue converted warm white light-emitting diodes. *J. Mater. Chem. C* **2019**, *7*, 247−255.
(32) Song, E.; Wang, J.; Shi, J.; Deng, T.; Ye, S.; Peng, M.; Wang, J.; Wondraczek, L.; Zhang, Q. Highly Efficient and Thermally Stable K_3AlF_6:Mn^{4+} as a Red Phosphor for Ultra-High-Performance Warm White Light-Emitting Diodes. *ACS Appl. Mater. Interfaces* **2017**, *9*, 8805−8812.
(33) Wang, L. Y.; Song, E. H.; Deng, T. T.; Zhou, Y. Y.; Liao, Z. F.; Zhao, W. R.; Zhou, B.; Zhang, Q. Y. Luminescence properties and warm white LED application of a ternary-alkaline fluoride red phosphor K_2NaAlF_6:Mn^{4+}. *Dalton Trans.* **2017**, *46*, 9925−9933.
(34) Yi, X. D.; Li, R. F.; Zhu, H. M.; Gao, J.; You, W. W.; Gong, Z. L.; Guo, W.; Chen, X. Y. K_2NaAlF_6:Mn^{4+} red phosphor: room-temperature synthesis and electronic/vibronic structures. *J. Mater. Chem. C* **2018**, *6*, 2069−2076.
(35) Deng, T. T.; Song, E. H.; Sun, J.; Wang, L. Y.; Deng, Y.; Ye, S.; Wang, J.; Zhang, Q. Y. The design and preparation of the thermally stable, Mn^{4+} ion activated, narrow band, red emitting fluoride Na_3GaF_6:Mn^{4+} for warm WLED applications. *J. Mater. Chem. C* **2017**, *5*, 2910−2918.
(36) Ming, H.; Liu, L. L.; He, S. A.; Peng, J. Q.; Du, F.; Fu, J. X.; Yang, F. L.; Ye, X. Y. An ultra-high yield of spherical K_2NaScF_6:Mn^{4+} red phosphor and its application in ultra-wide color gamut liquid crystal displays. *J. Mater. Chem. C* **2019**, *7*, 7237−7248.
(37) Deng, T. T.; Song, E. H.; Zhou, Y. Y.; Wang, L. Y.; Ye, S.; Zhang, Q. Y. Stable narrowband red phosphor K_3GaF_6:Mn^{4+} derived from hydrous $K_2GaF_5(H_2O)$ and K_2MnF_6. *J. Mater. Chem. C* **2017**, *5*, 9588−9596.
(38) Zhu, Y. W.; Chen, D. Q.; Huang, L.; Liu, Y.; Brik, M. G.; Zhong, J. S.; Wang, J. Phase-transition-induced giant enhancement of red emission in Mn^{4+}-doped fluoride elpasolite phosphors. *J. Mater. Chem. C* **2018**, *6*, 3951−3960.
(39) Jiang, C. Y.; Brik, M. G.; Li, L. H.; Li, L. Y.; Peng, J.; Wu, J. N.; Molokeev, M. S.; Wong, K. L.; Peng, M. Y. The electronic and optical

https://doi.org/10.1021/acsmaterialslett.4c00263
ACS Materials Lett. 2024, 6, 1790−1800

properties of a narrow-band red-emitting nanophosphor $K_2NaGaF_6:Mn^{4+}$ for warm white light-emitting diodes. *J. Mater. Chem. C* **2018**, *6*, 3016−3025.

https://doi.org/10.1021/acsmaterialslett.4c00263
ACS Materials Lett. 2024, 6, 1790−1800